Robotic Millimeter-Wave Wireless Networks

Anfu Zhou, *Member, IEEE*, Shaoqing Xu, Song Wang, Jingqi Huang, Shaoyuan Yang, Teng Wei, Xinyu Zhang, *Associate Member, IEEE*, and Huadong Ma, *Senior Member, IEEE*

***Abstract*— The emerging millimeter-wave (mmWave) networking technology promises to unleash a new wave of multi-Gbps wireless applications. However, due to high directionality of the mmWave radios, maintaining stable link connection remains an open problem. Users' slight orientation change, coupled with motion and blockage, can easily disconnect the link. In this paper, we propose RoMil, a robotic mmWave relay that optimizes network coverage through wireless sensing and autonomous motion/rotation planning. The robot relay automatically constructs the geometry/reflectivity of the environment, by estimating the geometries of all signal paths. It then navigates itself along an optimal moving trajectory, and ensures continuous connectivity for the client despite environment/human dynamics. We have prototyped RoMil on a programmable robot carrying a commodity 60 GHz radio. Our field trials demonstrate that RoMil can achieve nearly full coverage in dynamic environment, even with constrained speed and mobility region.**

***Index Terms*— 60 GHz mmWave networks, mobile relay, user tracking, path planning.**

I. Introduction

THE past few years have witnessed major evolution of ultra-high-speed millimeter-wave (mmWave) networks. While originally designed for quasi-stationary use cases such as cellular backhaul [1], wireless datacenters [2], [3] and wireless display [4], mmWave networks are anticipated to become mainstream in 5G, and enable much more versatile applications, including WiFi-like access, untethered virtual reality, mobile offloading, *etc.* [5]. However, the inherent shortcomings of mmWave links, *i.e.*, limited coverage and stability, remain a major barrier in practice. Although a mmWave radio can use phased-array antennas to generate highly directional, electronically steerable beams, the joint coverage of all its beams can only form a limited Field of View (FoV) (typically below 170° [6]) just like a camera lens. As a result, it is non-trivial to maintain stable link connectivity even at a room-level.

Manuscript received April 25, 2019; revised December 15, 2019; accepted April 6, 2020; approved by IEEE/ACM TRANSACTIONS ON NETWORKING Editor T. He. Date of publication May 19, 2020; date of current version August 18, 2020. This work was supported in part by the National Key Research and Development Program of China under Grant 2019YFB2102202, in part by the National Natural Science Foundation of China (NSFC) under Grant 61772084, Grant 61720106007, and Grant 61832010, in part by the Funds for Creative Research Groups of China under Grant 61921003, in part by the 111 Project under Grant B18008, and in part by the Fundamental Research Funds for the Central Universities under Grant 2019XD-A13. *(Corresponding author: Huadong Ma.)*

Anfu Zhou, Shaoqing Xu, Shaoyuan Yang, and Huadong Ma are with the Department of Computer Science, Beijing University of Posts and Telecommunications, Beijing 100876, China (e-mail: zhouanfu@bupt.edu.cn; donggua@bupt.edu.cn; yangsy@bupt.edu.cn; mhd@bupt.edu.cn).

Song Wang, Jingqi Huang, and Xinyu Zhang are with the Department of Electrical and Computer Engineering, University of California at San Diego, La Jolla, CA 92093 USA (e-mail: sowang@ucsd.edu; jih032@ucsd.edu; xyzhang@ucsd.edu).

Teng Wei is with the Department of Electrical and Computer Engineering, University of Wisconsin-Madison, Madison, WI 53706 USA (e-mail: twei7@wisc.edu).

Digital Object Identifier 10.1109/TNET.2020.2990498

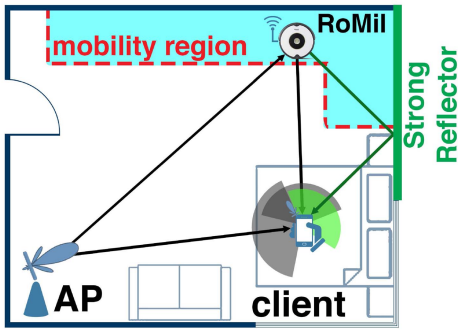

Fig. 1. Usage scenario of RoMil.

Link outage often occurs when a user exits the access point's FoV due to motion, hand/body rotation, or blockage by other surrounding people.

To overcome the challenge, one natural method is to deploy relays with complementary FoVs to approximate pervasive coverage [6], [7]. However, our field tests reveal that the effectiveness of mmWave relaying highly depends on the environment and device locations, and a static relay still suffers from many blind zones/angles (Sec. II). Although deploying multiple APs may help, it has been shown that even 3 APs can only cover 90% of a simple $7 \times 8\ m^2$ area without any human activities nearby [6]. Worse still, the blind zones/angles vary dynamically as more people walk around, thus demanding more APs to remove the blockage/shadowing effects. The resulting backhaul or cabling cost thus becomes formidable, even for a simple multi-room office or home environment.

In this paper, we propose RoMil, which explores robotic intelligence to realize continuous coverage for mobile mmWave users. RoMil is inspired by the vision that robots will eventually become part of the home and enterprise environments to help automate our daily lives and improve productivity [8]. In fact, cleaning robots [9] and telepresence robots [10] have already been widely adopted, promising a multi-billion market [11]. RoMil piggybacks a mmWave radio on a robot and transforms it into a mobile relay (Fig. 1). A naive way of leveraging this robotic relay is to always navigate it to "follow" the client. But this is infeasible in practice due to the robot's *limited moving speed/agility* and *constrained mobility region*, and when multiple clients coexist. The key insights behind RoMil are: *(i)* The mmWave channel is intrinsically sparse [12]. Coverage issue is often due to specular reflections not being redirected to the proper angle. Even minor movement of the robot relay can save the client out of the shadowed region. Therefore, it can improve the coverage substantially even under speed/space constraints. *(ii)* The client's orientation may change rapidly, and it is infeasible for the robot to keep itself within the client's FoV. However, if the mmWave robot can sense ambient

reflectors (*e.g.*, walls and furniture), it can judiciously navigate itself to a position/angle that may lead to a diverse set of reflection paths, thus probabilistically maximizing the *likelihood* of covering the client at any time. These insights set RoMil apart from the legacy WiFi or cellular relay networks [13], [14], whose designs are oblivious of node orientation and environmental structures.

Realizing the principle of autonomous mmWave relaying requires a revisit of two classical problems in robotics: environment mapping and path planning. Unlike the conventional robotic navigation, however, the unique challenge is that both problems need to be studied within the radio "environment" from the mmWave radios' eyes (comprised of the invisible signal paths and beams), rather than the physical environment. *First of all*, RoMil needs to predict the best feasible relay position based on prior knowledge of ambient reflectors, which in turn requires a reconstruction of the environment (*e.g.*, reflectivity and geometrical layout). At run time, the relay can keep tracking the client's position, and plan its moving trajectory to maximize the likelihood of full coverage for the client. Reconstructing the environment requires disentangling each reflection path and characterizing each reflecting point. Conventional ways of resolving signal paths [15], *i.e.*, discriminating their angle-of-arrival (AoA) and angle-of-departure (AoD), require phase-coherence across packets, which is infeasible on commercial-off-the-shelf (COTS) mmWave communication devices [16]. In RoMil, we propose a beam spatial correlation maximization method, which combines the autonomous motion control and self-localization capability of the robot, with simple RSS measurement from the mmWave radio, to extract the path geometries. Then we build a geometrical model to transform the path information into an environment outline. Meanwhile, we leverage the diversity of phased-array beam patterns, to enable a single relay to track the client's position even under blockage.

Second, the path planning for mmWave relay is intrinsically dynamic, and differs fundamentally from conventional path planning algorithms in robotics and robot-driven omni-directional radio networks [17]–[19]. Legacy path planning derives the shortest/optimal path to *one or more target positions*. But the mmWave relay needs to maintain high link performance for the client *along the path*. This implies the relay needs to predict the client's performance along each point of the path, which is non-trivial as the performance depends on the environment, as well as the relative position/orientation between the relay, client and AP. Moreover, even for an oracle with perfect prediction, computing the optimal trajectory across the points entails exponential complexity. In RoMil, we introduce a statistical method to predict the relay performance; We then simplify the relay path planning as a tree searching problem, based on an undiscovered *locality* property of the relay's spatial performance distribution.

RoMil, to our knowledge, represents the first system that harnesses robotic intelligence to facilitate seamless mmWave networking. Its contributions can be summarized as:

(i) We design novel algorithms that combine the motion/orientation control capability of the robot with the RSS measurement capability of COTS mmWave radios, to accurately recover the geometries of signal paths, and subsequently create an outline of the environment from the mmWave radios' eyes.

(ii) We design an adaptive path planning algorithm that navigates the robot relay in real-time, and statistically maximizes network performance under environment dynamics and the client's self-blockage.

(iii) We implement RoMil on a programmable robot, integrated with COTS 802.11ad radios. Our experiments in multi-room environments verify that RoMil can maintain nearly full coverage for an office environment, even when the robot is constrained to a small area and low speed. In comparison, existing solutions need around 4-5 APs to achieve similar performance.

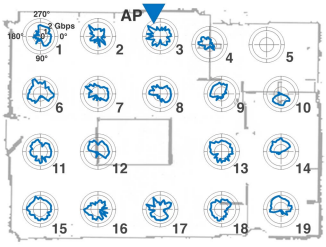

Fig. 2. Client throughput across all orientations and at 19 locations.

II. Measurements and Motivation

We now conduct experiments to elucidate the challenges of achieving multi-room coverage, and the effectiveness of an optimally navigated robotic relay. We will then design RoMil to approach this ideal (Sec. III to Sec. VI). Our experiments run in a typical $8 \times 10\ m^2$ office with multiple cells, separated by concrete walls, as shown in Fig. 2. We put the AP near a wall, facing the interior. We then attach an 802.11ad radio to a robot to represent either a relay or a client with controlled mobility (more implementation details in Sec. VII). For each location that the robot dwells on, we program the robot to rotate over $360°$ in steps of $3°$. At each angle, we measure the AP-robot link's TCP throughput after the 802.11ad MAC level *beam searching* stabilizes (which has proven to converge to the best available beam within the phased-array's FoV [6]). We refer to each set of such measurement results as *circular throughput* at a specific location. We have two major observations from the measurement.

Observation 1 Ineffectiveness of Fixed AP and Relay: *A static AP, even when combined with a fixed relay, cannot provide omni-directional reliable coverage.*

In Fig. 2, we plot the circular throughput of 19 evenly distributed locations. For most locations, a client experiences extremely low throughput when it faces several blind angles. More critically, location 5 lies in a blind zone, suffering from link outage along all angles. To quantify the robustness of network performance to client's orientation changes, we define a ρ-factor as: $\rho = \tilde{D}/D$, where $\tilde{D}$ is the number of directions with throughput exceeding a certain threshold, and D is the total number of rotation angles (*i.e.*, 120). Here the threshold is set to be half of the maximum throughput over all D directions. Clearly, a higher ρ ($0 \leq \rho \leq 1$) implies that the link is more resilient against the device's angular variations.

Fig. 3 summarizes the ρ-factor distribution across all 19 locations. Intuitively, ρ should be less than 0.5 since the antenna FoV is below $180°$. However, over 60% locations measure $\rho > 0.5$. The gain is brought by non-line-of-sight (NLoS) reflections from strong reflectors (concrete walls, whiteboard, *etc.*). For instance, reflection helps to achieve almost full circular coverage for the client at the corner

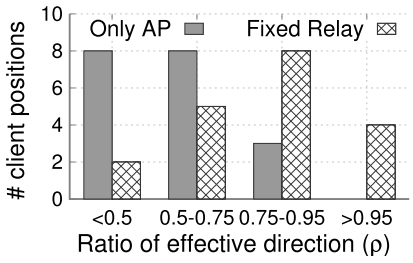

Fig. 3. Effect of a fixed-relay.

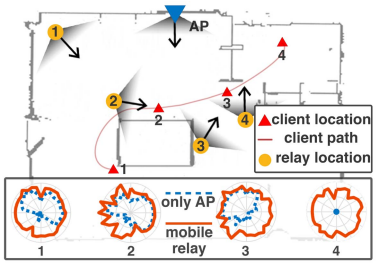

Fig. 4. Potential of a mobile relay.

location 15. The result implies that *whether full coverage can be achieved heavily depends on how the reflectors are leveraged*.

To quantify how useful a relay is, we intentionally place a relay on the wall opposite to the AP, since this position shall provide the most complementary FoV. Then we measure the *throughput* of the relay-assisted link, *i.e.*, the maximum of the AP-client link vs. AP-relay-client link for each client orientation. Fig. 3 plots the ρ factor distribution in contrast to the AP-only case. Although ρ sees notable improvement, there still exist 37% (10%) locations with $\rho < 0.75$ ($\rho < 0.5$), and the blind zone around location 5 persists. We have also tried many other relay positions, but the effect remains the same: a fixed relay improves the performance of some client locations, whereas the remaining blind zones/angles can still disrupt the connectivity.

Observation 2 Potential of an Autonomous Mobile Relay: An ideal mobile relay can remove blind zones/angles, and maintain omni-directional coverage even for mobile users.

We now evaluate the effectiveness of a mobile relay, assuming it can navigate to the optimal position according to the client location. Fig. 4 illustrates the experimental scenario. We pick 4 locations along a client's moving trajectory. For each location, we select the optimal relay position & orientation (through exhaustive trial comparisons) and measure the circular throughput. The results demonstrate significant gains from a mobile relay: the optimal relay provides an omni-directional high throughput for every client location, even for location 5 originally in the blind zone.

One may consider using *multiple APs/relays*. However, static APs/relays, with fixed FoVs, can hardly accommodate the orientation/blockage dynamics. Our tests (Sec. VIII-B) will show that, to remove majority of the blind zones/angles in a small $14 \times 16\ m^2$ area, as many as 5 APs are needed! And even 10 APs cannot fully remove the coverage holes near corners. In contrast, a single RoMil relay, even with limited speed and constrained mobility region, achieves similar or even better performance.

Despite the tremendous potential, making the mobile relay autonomous and optimal entails multiple practical challenges,

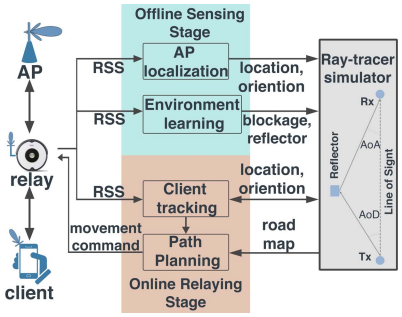

Fig. 5. RoMil system modules and work flow.

i.e., learning and exploiting the environment, tracking the client, and planning the relay's moving path. In what follows, we present our design to meet these challenges.

III. RoMil Operations

RoMil's operations follow two stages, as illustrated in Fig. 5. When entering a new environment, RoMil needs to initialize itself through an *offline sensing stage*. Here the robotic relay roams around and locates the AP relative to a prescribed starting point, by simply sampling the AP-to-relay RSS. Then the relay, assisted by the AP, reconstructs the environment, *i.e.*, inferring location, shape and reflectivity of major reflectors and obstacles. Both the AP location and environment information is fed into a ray-tracing engine, which models the signal's propagation and interaction with environment, thus enabling RoMil to *predict the channel quality of arbitrarily located AP-client or AP-relay-client links*.

Afterwards, during the *online relaying stage*, the relay keeps tracking the client, based on prior knowledge of the environment, and the RSS of the relay-client link (for LOS and/or NLOS signals). Further, the relay employs an *adaptive path planning* scheme to *compute the optimal moving trajectory*, and roams itself accordingly. To handle the "cold start" issue (*i.e.*, during boot time, the relay fails to find the client due to long link distance or blockage), the relay identifies and attempts a minimal set of *backup positions*, which can cover the unknown client location with high probability.

To simplify the exposition, we mainly focus on the scenario with single AP and client. But RoMil can be easily extended to multi-client scenarios with customized fairness policies and even to multi-relay scenarios (Sec. VIII-A.5).

IV. The Offline Sensing Stage

Modern consumer robots, equipped with optical rangers, motion sensors, and SLAM algorithms, can already achieve self-localization and floor map reconstruction [9], [20]. But they are unaware of mmWave signals' propagation/reflection/penetration in the environment, which determines the relay performance. RoMil augments the robot's physical sensing with mmWave wireless sensing. The core mechanism behind is called beam-cross-section correlation maximization (BCS-CM). BCS-CM extracts the embedded spatial information from a series of AP beacons, and then recovers the AoA/AoD of mmWave signal paths. Such signal path geometry, combined with the robot's view, creates a radio environment map which is the key input into RoMil's path planning algorithm.

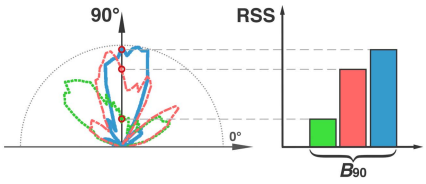

Fig. 6. Beam cross section.

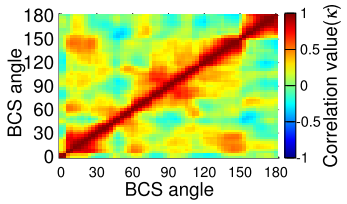

Fig. 7. BCS correlation.

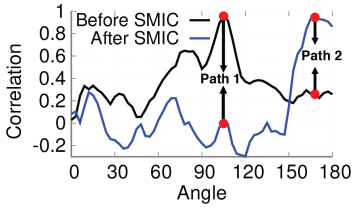

Fig. 8. Effect of SMIC.

A. Path Geometry Estimation Using BCS-CM

To estimate the path AoA/AoD, there are several design choices: *(i)* one naive solution is to treat the mmWave radios as directional laser scanners, and steer over all angles to locate the reflecting point, just like optical LIDAR. However, practical mmWave phased-array beam patterns have imperfect directionality and limited spatial resolution. The beamwidth can be very wide (more than 30° for most beams even for a 32-element phased-array [6]), and multiple strong side-lobes often coexist, which hampers accurate path estimation [6], [15], [21]. *(ii)* While many advanced AoA/AoD estimation methods have been proposed, most of the works (see [15], [22] and references therein) require coherent phase across beacons, which is unavailable in commodity mmWave devices. *(iii)* Rasekh *et al.* [16] designs the first non-coherent method for AoA/AoD estimation. While it can accurately estimate one major path, it cannot handle the case of co-existent multiple paths. *(iv)* To resolve co-existent multiple paths, a recent work Pia [6] proposes a pose-assisted compressive angle estimation method, based on a statistical optimization model. However, the method needs to solve a complicated non-linear constrained optimization problem, which involves high computational complexity.

Inspired by previous works on AoA/AoD estimation, particularly [22] and [16], BCS-CM solves the issue by harnessing redundant spatial information embedded in a series of beams. It can efficiently (*i.e.*, only basic arithmetic operations are needed) recover the AoA/AoD of multiple co-existing paths through a successive multi-path interference cancellation (SMIC) scheme, using only RSS measurement available on COTS devices. We now proceed to the details.

Beam Cross Section. The 802.11ad standard mandates that an AP (Tx) broadcasts a series of beacons in the beginning of each beacon interval to facilitate network discovery. The beacons are directional and bear unique beam patterns. The Rx is typically tuned to quasi-omni mode when trying to capture the beacons [6]. We define the *beam cross section* (BCS) as the set of RSS measured at a certain angle for all beacons. Fig. 6 illustrates the BCS of 3 beam patterns cut at 90° (relative to the antenna plane at 0°), measured on our 32-element 802.11ad radio (Sec. VII). Formally, suppose we discretize the 2D horizontal plane (perpendicular to the phased-array panel) into multiple angles then a BCS at angle i is denoted as B_i and defined as follows,

$$B_i = \{RSS_{1,i}, \cdot\cdot, RSS_{j,i}, \cdot\cdot RSS_{N,i}\} \tag{1}$$

where $RSS_{j,i}$ is the signal strength of j_{th} beacon at the i_{th} angle, and N is the number of beacons.

BCS Correlation Maximization (BCS-CM). Here for simplicity, we assume that there is only one signal path between Tx-Rx, and the AoD of the path is from the i_{th} direction (the assumption will be relaxed soon in the later SMIC). Then ideally a quasi-omni Rx will measure the vector B_i during Tx's beacon sweeping. These ideal B_i values can be derived during the phased-array's factory calibration, or from a one-time measurement of all its beam patterns (Sec. VII). In practice, BCS deforms due to signal attenuation and multi-path reflections, represented by an unknown channel gain h_i. The actual measured BCS (denoted with B^M, where the superscript M means "measured") should follow [6], [16]: $B^M = h_i B_i + n$ where n is the noise. Note that frequency selective fading may vary h_i across frequency bins in a wideband channel. But to simplify exposition, we can consider a typical frequency bin that represents the average across all bins.

To identify the underlying direction i from the measurement value of B^M, BCS-CM uses RSS trend in the BCS rather than absolute RSS values. Intuitively, BCSs are distinguishable due to the beam pattern heterogeneity across beacons. In Fig. 7, we compute and plot $\kappa(B_i, B_j)$, the correlation coefficient [23] of two BCS vectors (B_i and B_j) to measure their linear dependence, from which we observe that the correlation between two BCSs of different angles is much smaller than that of the same angle, *i.e.*, $\kappa(B_i, B_j) \ll \kappa(B_i, B_i)$. The result implies that BCS correlation is highly resilient to channel distortion. Therefore, we can compute correlation between measured B^M and each of the ideal B_i values, and pick the direction i^* corresponding to the maximum correlation as the AoD, *i.e.*,

$$i^* = \arg\max_i \kappa(B^M, B_i) \tag{2}$$

The AoA is derived using the same method, with a Tx-Rx role reversion. We omit the details due to space constraint.

Successive multi-path interference cancellation (SMIC). In practice, multiple paths may coexist between Tx and Rx, and the measured BCS may contain one or more B_i with diverse channel gains, expressed as:

$$B^M = \textstyle\sum_{i\in\Phi} h_i B_i + n \tag{3}$$

In this case, directly applying BCS-CM will result in erroneous AoD estimation. We illustrate this point using an example BCS measurement that comprises two paths: path 1 with AoD 105° and channel gain 0.8, and path 2 with AoD 168° and channel gain 0.3. Fig. 8 plots the correlation between measured BCS and possible B_i values. While BCS-CM can accurately identify path 1 (correlation peak), it cannot find path 2 whose correlation is immersed in noise.

To recover weaker paths, BCS-CM employs a SMIC design, inspired by successive interference cancellation [24], [25] in

Algorithm 1 Path Geometry Estimation

Input: all B_i for each i_{th} direction, measured B_M
Output: the set of AoD angles Φ
Initialization: $\Phi = \emptyset$, BCS residue $B_r = B_M$
while *Eq.* (6) *doest not hold* **do**
  /*paths remian to be detected*/
  Identify next path with angle i^* using Eq. (2);
  Compute channel gain h_i^* using Eq. (5);
  Update B_r using Eq. (4);
  $\Phi = \Phi \cup i^*$;
end

communication theory. SMIC first detects the strongest path through BCS-CM. It then subtracts that path's BCS from the measured BCS and reruns BCS-CM from the residue. The process iterates until all the paths are identified. Algorithm 1 summarizes this procedure.

Realizing SMIC entails two challenges: *(i)* After detecting a path with AoD along i_{th} angle, how should SMIC obtain the h_i to be canceled? *(ii)* When to stop SMIC's iterative process, given that the number of paths is unknown? We solve the problems by further exploiting the information embedded in BCS correlation. *First*, suppose we just detected a path with i_{th} angle using Eq. (2), the problem is to estimate its channel gain h' as accurately as possible, so we can get a purified residue B_r after canceling $h_i B_i$ from B^M, *i.e.*,

$$B_r = B^M - h'B_i = (h_i - h')B_i + \textstyle\sum_{j\in\Phi\&j\neq i} h_j B_j + n \tag{4}$$

From above, we can deduce that the absolute correlation between B_r and B_i will be minimized when $h' = h_i$. Thus, we can estimate channel gain h_i^* as follows,

$$h_i^* = \arg\min_{h'} |\kappa(B_r, B_i)| \tag{5}$$

where we limit h' within $(0, 1)$. After deciding on h_i^*, we will get an accurate residue B_r and keep the iterative SMIC going. Continuing with the example in Fig. 8, path 2's correlation peak appears after path 1 is canceled. *Second*, SMIC should stop when no path exists in B_r, when correlation approaches noise floor $\kappa(B_r, n)$. Formally, the stopping rule is:

$$\frac{\max_{\forall i} |\kappa(B_r, B_i)|}{mean(\sum_{\forall i} |\kappa(B_r, B_i)|)} \leq \sigma \tag{6}$$

Here the smaller the threshold σ, the more paths would be detected, but possibly with false positives. In practice, we find that $\sigma = 2$ suffices. This may miss some weaker paths (like the path with AoD around 70-80 degrees in Fig.6). However, such missing does not affect RoMil's environment sensing, which needs only stronger paths to provide more reliable information.

B. Environment Reconstruction

Locating the AP. RoMil achieves *fully automatic AP location and orientation sensing, by exploiting mobility and self-localization ability of the robot relay*. Specifically, the robot needs to roam randomly around the AP, and select L locations with the highest link throughput (most likely due to the existence of a LoS path). At each location $l \in [1, L]$, the robot derives the AoA of the strongest path, θ_l, using BCS-CM. Meanwhile, the robot relay knows its own position x_l.

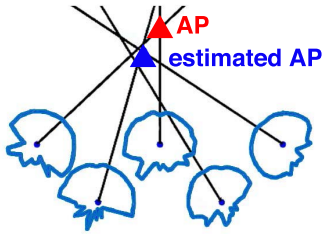

Fig. 9. AP localization.

Given x_l and θ_l, RoMil runs a statistical method to estimate the *AP location*, illustrated in Fig. 9: corresponding to each x_l, the angle θ_l indicates the possible direction of the AP relative to the robot. In total there exist $L(L-1)/2$ intersection points among all L possible directions. We use the center of all intersection points, x_{AP}, as the final estimation. Similarly, we derive *AP orientation* by examining all possible AP orientation $0 \leq \alpha \leq 360$. Specifically, since the radios' beam patterns are known *a priori*, we can predict a BCS received at each relay position given x_{AP} and an α. Then we try each α and find the one with the prediction closest to the actual BCS measured by the robot. To minimize errors, we use the average orientation estimation over all L robot locations.

Locating reflectors and constructing environment map. RoMil reconstructs an outline of the environment by combining robotic motion and mmWave sensing. By sweeping through the space, the robot first generates an environment floor map. Meanwhile, given the AoA and AoD of all NLoS signal paths (obtained through BCS-CM), the robot can locate the points that reflect ("bend") the mmWave signal paths, using classical geometrical models [15]. RoMil then corrects the location error by matching each reflecting point to the closest point on the floor map. Furthermore, it estimates the reflection loss of each point, by subtracting the measured channel gain along the NLoS path from the ideal Friis LoS path loss. Similarly, it can estimate the penetration loss when the robot roams behind an obstacle. Following these steps, RoMil creates a map of the environment from the mmWave radios' "eyes". Note that for multi-room environment, to facilitate environment learning, the AP may need to be temporarily moved to multiple locations (but no backhaul is needed) so that its signals can hit all reflectors.

Using the learned information to drive ray-tracing. The ultimate link quality between the AP, relay and client depends on the radio beam patterns, signal propagation loss, and environmental distortion (reflection and penetration loss). We model such joint effects through a ray-tracing approach, which uses environment information (*i.e.*, AP location, reflector layout/reflectivity, blockage layout/penetration), and the measured beam patterns of each mmWave radio, as input; and outputs the RSS accordingly. Our ray-tracer follows the classical process in [15], whose accuracy has been extensively validated.

We note that some machine learning based methods (see [26], [27]) have recently been proposed for predicting channel quality. They may help to improve prediction accuracy of RoMil, and even removes the environment mapping stage that is currently necessary in RoMil. We leave such exploration to future work.

V. Client Tracking

Client tracking is much like AP-localization. To track the client's location, the relay first derives the measured BCS

between itself and the client. It then employs the ray-tracer to compute the BCS of each possible candidate location, and picks the one that best matches the measured BCS (*i.e.*, with the maximum correlation). Here the time consuming ray-tracing process (*i.e.*, predicted BCS between any pair of relay and client) is done *offline* and cached as a look-up table. Note that human dynamics can also be processed offline by enumerating BCSs under all possible combinations of path blockage and client orientation. So at run time, RoMil only needs to run a simple correlation-match computation to enable real-time client tracking. We emphasize that the searching space of the path blockage-orientation combination is limited: *(i)* In RoMil, we use at most 3 strongest paths for environment mapping and client tracking, due to the mmWave's channel sparsity. Then the overall number of possible blockage combination is $2^3 = 8$. *(ii)* We use an angle resolution of 3° when enumerating client orientation change, and the resulting number of orientation choices equals to $\frac{360^\circ}{3^\circ} = 120$. As a result, the size of choice space for the correlation-match is $120 * 8 = 9600$. During the match process, only basic arithmetic operations are needed s, and the overall latency is less than 10ms for RoMil making each decision in our current prototype implementation (Sec. VII).

However, *location ambiguity* may arise, *i.e.*, more than one candidate locations may have similar path geometries. It is mentioned that only strongest 2 or 3 paths may impact BCS, the number of path blockage and client orientation combinations would not grow too large. Consequently, the simple correlation-match procedure would only take a short time. RoMil resolves the ambiguity by exploiting the continuity of client's movement. Among all candidate locations that match the measured BCS, it picks the one closest to the latest client location sample. We emphasize that *RoMil's client tracking works regardless of client orientation or blockage*. This is because its BCS correlation match takes into account all possible LoS and NLoS paths between the relay and the client. Even if certain paths are blocked by other users or the client herself, other paths may still survive and lead to the highest correlation.

VI. Adaptive Path Planning

To execute the path planning, we design a statistical performance indicator called *E-index*, to quantitatively characterize how good a relay position & orientation is, based on the learned environment information. For a given client position, the relay's E-index distribution over space is called a *roadmap*. Then we model the relay path planning as a tree searching problem on the roadmap. We further exploit a 'locality' property of relay performance to reduce the model complexity, and design a practical adaptive path planning scheme for mobile client (*i.e.*, dynamic roadmaps). We now describe each design component in detail.

A. E-index to Model Relay Performance

A straightforward way to determine optimal relay position is to find the one that brings the maximum signal strength for the client. However, though this solution may have the highest performance for a static user, it will fail when client users rotate or are blocked by other people. For instance, when a client user turns to the opposite direction, the strongest signal path may be blocked by the user's own body. In theory, a robot can find another location to maximize the RSS again, but in practice, the robot can not move fast enough to catch the user's rotation speed. Therefore, a good relay position should enhance the client's resilience against rotation or blockage. Intuitively, a better relay position should manifest two characteristics: *(i)* The relay→client paths' AoAs should be sparsely distributed across all angles, and should be complementary to the AP→client paths', so that the *likelihood* of all paths being simultaneously blocked is low. *(ii)* Both the AP→relay and relay→client links should have strong RSS to ensure high throughput across the two hops.

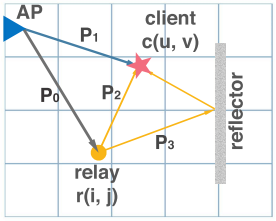

Fig. 10. Cell decomp.

The *E-index* metric incorporates the two characteristics, drawing on inspiration from the entropy concept in information theory [28]. Consider an arbitrary relay location and orientation which, together with the AP, creates P signal paths to a client, each path with RSS β_p and AoA ϕ_p ($\forall p \in [1, P]$). We denote the corresponding spatial channel profile as $\Psi = \{(\beta_1, \phi_1), (\beta_2, \phi_2), \ldots, (\beta_P, \phi_P)\}$.

To examine the AoA's spatial distribution, we split the horizontal space into S angular zones, $A_s, \forall s \in [1, S]$. For each zone, we define its *zone RSS* as the sum signal strength of all paths falling in the zone, *i.e.*,

$$RSS_s = \sum_{\forall p, \phi_p \in A_s} \beta_p \tag{7}$$

Then we normalize the zone RSS by dividing each RSS_s by the total RSS, *i.e.*, $sumRSS \triangleq \sum_{s=1}^{S} RSS_s$, as follows,

$$\hat{RSS}_s = RSS_s / sumRSS \tag{8}$$

Treating $\hat{RSS}_s, \forall s \leq S$ as a sequence of numbers that form a probability density function, we characterize how evenly the zone RSS are distributed across all angles, following the entropy definition, *i.e.*,

$$eRSS = \sum_{s=1}^{S} \hat{RSS}_s \times \log(1/\hat{RSS}_s) \tag{9}$$

Then the *E-index* η is defined as follows,

$$\eta = sumRSS \times eRSS \tag{10}$$

where $eRSS$ reflects AoA sparsity to keep resilience to rotation/blockage, and *sumRSS* reflects the need for strong RSS. In other words, η considers not only absolute RSS (*sumRSS*) which ensure high quality link, but also path diversity (*eRSS*) which increases robustness under environment/human dynamics.

Computing the spatial distribution of E-index. Note that the E-index η depends on the positions of the client and relay, and also the surrounding environment. To formalize the relationship, we first *discretize the space* into $M \times N$ cells, as shown in Fig. 10. We define C_0, C_1 as the set of cells that relays or clients can move freely, respectively. Note that C_0 can be any constrained region defined by end-users

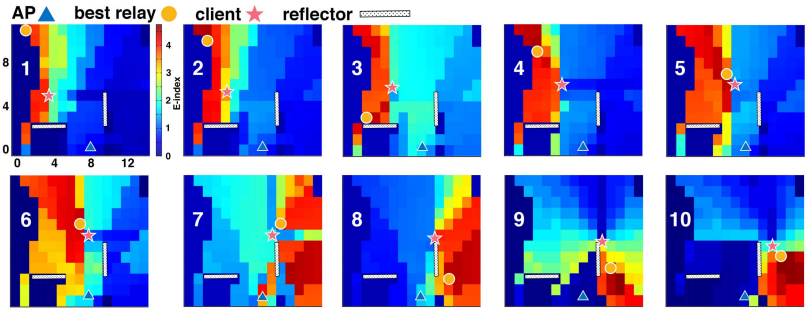

Fig. 11. Relay locality: bright (red) color represents high E-index.

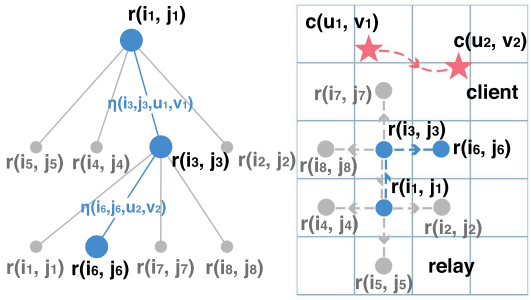

Fig. 12. Tree model.

(*e.g.*, limited to within 0.5m against walls as in our experiments in Sec. VIII-B), so that the relay will *not* interfere with human daily activities. Given any pair of relay and client, located in cell (i, j) and (u, v) respectively, we can derive the signal path geometries and RSS for the client following Sec IV. We then compute the E-index for the pair, $\eta(i, j, u, v)$, using Eq. (10). For a given client position (u, v), we denote the spatial distribution of E-index across all possible relay positions (i, j) as a *roadmap*.[1]

Determining the optimal relay position. For a client position $c(u, v) \in C_1$, the optimal relay position $r(i^*, j^*)$ can be derived as

$$(i^*, j^*) = \underset{\forall r(i,j) \in C_0}{\arg\max}\ \eta(i, j, u, v) \tag{11}$$

Fig. 11 plots the roadmaps as a client moves across 10 locations in an example scenario. The optimal relay positions within each roadmap are highlighted. We can observe the unique challenges in navigating the robotic mmWave relay. In particular, the *legacy path planning algorithms* (*e.g.*, A^*, D^*, *etc.* [29], [30]) navigate a robot along the shortest feasible path. But they cannot guarantee network performance of the points along the path, which is critical for mmWave connectivity. Moreover, the *roadmap keeps changing* after each movement of the client, which renders legacy path planning infeasible.

B. Tree Model Over Dynamic Roadmap

To handle dynamic roadmaps and ensure intermediate relay performance, we build a tree searching model, as illustrated in Fig. 12. The root is the initial relay position; the children nodes are its reachable neighboring cells, and the edge weight is the E-index of the corresponding child. In this way, we essentially model roadmap dynamics (*i.e.*, varying E-index) through different E-index weight at different tree depth. For instance, if the relay plans to move from the root $r(i_1, j_1)$ to $r(i_3, j_3)$ at depth-1, the edge weight is $\eta(i_3, j_3, u_1, v_1)$ given the current client location $c(u_1, v_1)$. Suppose the client also moves to a new location $c(u_2, v_2)$ as the relay moves to $r(i_3, j_3)$, then the edge weights to depth-2 nodes will be the E-index when the relay moves to $r(i_3, j_3)$'s neighbors, *e.g.*, $\eta(i_6, j_6, u_2, v_2)$, if the relay plans to move to $r(i_6, j_6)$ for the next step.

From an oracle's perspective, the optimal relay path can be derived using a brute-force tree searching, assuming the client's trajectory is known *a priori*. However, two challenges arise in practice: *(i)* Predicting client movement is a non-trivial and error-prone task. *(ii)* The search complexity is $O(P^d)$, where P is the cardinality of children (*i.e.*, 4 if we limit the robot to straight-line movement), and d is tree depths (hundreds to thousands scale). Clearly, the computational cost and resulting delay is unaffordable.

C. Adaptive Tree Searching by Harnessing E-Index Locality

RoMil curtails the path planning complexity through an adaptive tree searching (ATS) algorithm, which harnesses a "locality" property of E-index. As illustrated in Fig. 11, positions with high E-index tend to form a cluster (henceforth referred to as *good-zone*). Relay performance is consistently high inside the zone. More importantly, the good-zone moves forward gradually along with client movement, until an abrupt environmental change (*e.g.*, the client passes a major obstacle, such as a large TV screen, shown in subplot 7). Afterwards, a new good-zone forms and the phenomenon repeats (*i.e.*, subplot 7, 8, 9 and 10). In fact, the locality property roots in the spatial channel sparsity inherent to mmWave channels. Specifically, for a given client position, a few major signal paths dominate the performance, whereas the path strengths and incident angles gradually evolve with user mobility, unless sudden environmental change blocks the paths and/or creates new ones. We can also observe that a good-zone commonly includes many cells, which hints that RoMil robot may find near-optimal location to move to *even if it is constrained to a certain mobility region*.

The *locality of E-index implies that short-depth tree searching suffices, based on short-term prediction of user movement*. Accordingly, ATS operates as follows. (Algorithm. 2). *(i)* It estimates K time slots of client user's future movement using first-order prediction, *i.e.*, For each $1 \le k \le K$ slot, the predicted client location is:

$$c_k = c_0 + v_0 * T_k \quad \forall k < K \tag{12}$$

[1]Note that the relay's orientation, more specifically the on-board phased-array's orientation, also matters here. A qualified relay orientation should be inside the AP's FoV and is able to exploit reflections. RoMil always chooses the orientation creating the maximum E-index for the relay-client pair as the relay's orientation.

Algorithm 2 Adaptive Path Planning Algorithm

Input: current client location c_0 and velocity v_0
Output: movement command to the robot
while *True* **do**
  Predict K client locaions $\{c_1, \ldots c_K\}$ using Eq. (12);
  Derive roadmaps $\{f(1), \ldots f(K)\}$;
  Derive $\lambda(k)$, $\mu(k)$ of each $f(k)$'s good relay zone;
  if *Eq.* (13) *holds* **then**
    /*the optimal relay is nearby*/
    Search K depth over the tree model;
    Derive the optimal K-step relay path, $p*$;
    Command the relay move one step along $p*$;
  end
  else
    /*the optimal relay is far away*/
    Compute the optimal relay with max. E-index;
    Derive the optimal path using Dijkstra algo.;
    Command the relay moving along the path;
  end
  update c_0 and v_0 at the new relay position;
end

where c_0 and v_0 are the client's current location and velocity, and T_k is the time from now to k. Here we set $T_k = k * BI$, where BI is the beacon interval (typically below 100 ms) during which client localization executes. v_0 is calculated from previous client localization results, *i.e.*, the difference between the client's latest location and the last one. In Eq. (12), we use v_0 to predict the client's future location, assuming that client velocity keeps constant during next K consecutive beacon intervals. Note that one beacon interval lasts 100ms, and K is set to be 3 following our experimental observation in Fig. 22. So the assumption is reasonable in such a short time of 300ms. *(ii)* For each slot, ATS computes the relay's good-zones, and checks whether the zones experience a sudden shift. We detect a shift by examining how far the good-zones of consecutive roadmaps are separated from each other. Specifically, for two consecutive roadmaps denoted with $f(k)$ and $f(k+1)$, ATS derives the good-zone centers ($\lambda(k)$ and $\lambda(k+1)$) and radius ($\mu(k)$ and $\mu(k+1)$), using the classical clustering algorithm [31]. It then examines whether the L-1 distance of the centers is larger than the average radius, *i.e.*,

$$|\lambda(k+1) - \lambda(k)| \leq \frac{\mu(k+1) + \mu(k)}{2}, \quad \forall k < K \qquad (13)$$

If Eq. (13) holds, the relay will search the tree for K steps, and derive an optimal moving trajectory. To minimize the effect of wrong prediction, the relay moves only one step along the trajectory, then it repeats the K-step-prediction & one-step-movement procedure. If Eq. (13) does not hold, then zone shift happens. The relay will be aware that the optimal relay position is far away. Then it computes the optimal relay with the maximum E-index according to Eq. (11), and moves towards it along a path computed from the Dijkstra algorithm. Though Dijkstra algorithm cannot guarantee path optimality, in this case the priority is to reach the new good-zone as soon as possible. Also, note that user movement prediction at sub-second level is of high reliability [6]. Our evaluation result (Sec. VIII) will further show that 3 look-ahead steps ($K = 3$) already lead to high relay performance. In this way, the computational complexity is reduced significantly. At the best case, the complexity is only $O(P^K)$ ($P = 4$ and $K = 3$) when the locality property holds true. On the other hand, the complexity at the worst case becomes $O(N^2)$ (N is the number of cells of the roadmap) when ATS invokes the Dijkstra algorithm. The ratio between the two cases depends on the environment. The more complicated the environment, the more frequent the Dijkstra algorithm will be invoked. From our experimental observation, the ratio is about 10:1 in typical offices like the one in Fig. 2.

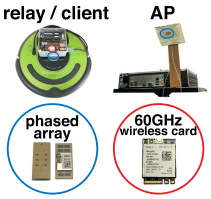

Fig. 13. RoMil prototype.

D. Determining the Backup Set

The "cold start" issue occurs at boot time, or when the relay suddenly loses track of the client. To handle this issue, RoMil prepares a backup set consisting of a few relay positions to satisfy two requirements: *(i)* The backup positions in combination shall cover the whole space, so that RoMil can guarantee to re-locate the client after the relay traverses the positions in the backup set. *(ii)* The traversal length (*i.e.*, the length of the shortest line connecting all backup points) shall be minimized so as to reduce re-locating latency. To identify the backup set, we formulate a constrained optimization problem. Suppose $\Omega \subset C_0$ represents a possible backup set, and $d(\Omega)$ is the traversal length of all positions in Ω. Then the optimization can be formulated as:

$$\begin{aligned} &\min_{\Omega}\ d(\Omega) \\ &\textit{s.t.}\quad \max_{(i,j)\in\Omega}\ \eta(i,j,u,v) \geq \zeta, \forall (u,v) \in C_1 \end{aligned} \qquad (14)$$

where ζ is the E-index threshold to guarantee strong link quality from the relay to the client. In theory, Ω can be any subset of C_0, which is a formidable search space, even though we can solve Eq. (14) offline. We thus limit $|\Omega| < 5$ in our system, which already achieves satisfactory performance as will be verified through experiments (Sec. VIII-A).

VII. Implementation

Hardware components. Our RoMil system prototype consists of an AP, relay and client, as depicted in Fig. 13. The AP is a small PC mounted on top of a tripod of 1.8m-height, and the relay and client are Intel NUC mini-PCs (around 4 inches on all dimensions) [32], mounted on Create 2 programmable robots [33]. The client device is at a user height (between 1 to 1.5m), while the relay robot is on the floor. These devices are all equipped with the Qualcomm 60 GHz network interface card [34], comprised of QCA6310 RF front-end, QCA6320 MAC/baseband, and a 32-element phased array (supporting 36 beams). As shown in the figure, the backside of the phased array is grounded by a metal plane, by following the common practice: the phased array is commonly installed close to the outer surface of the lid on COTS laptops like Acer P446 and Dell Latitude E7240. For smart-phones, phased arrays are usually placed on the bottom or top surface [35].

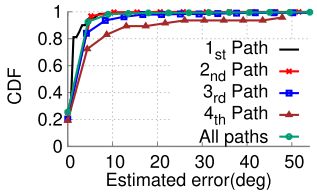

Fig. 14. Path estimation error.

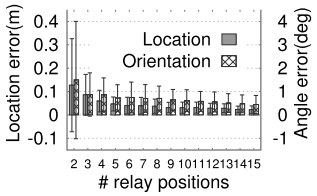

Fig. 15. AP estimation error.

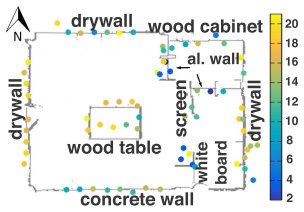

Fig. 16. Environment learned by RoMil.

TABLE I
ENVIRONMENT MAPPING STATISTICS

Object	Pos. est. error	Reflecttion loss (dB)
concrete wall	0.047m	12.390
west drywall	0.065m	18.169
north drywall	0.140m	13.520
east drywall	0.261m	15.226
al. wall	0.136m	8.791
screen	0.364m	12.682
white board	0.346m	7.657
table	0.371m	16.373

In these setups, the backside of the phased-array faces inward the host device which causes strong attenuation. As a result, the FoV is limited below 170 degrees, different from the beam patterns in previous works of [36], [37].

The NUC controls the robot through maneuvering commands (*e.g.*, translation/rotation directions, speed and duration). The commands for the relay robot follow RoMil's path planning algorithm, whereas the client robot is programmed to move freely like a vanilla user.

RoMil can either use the decode-and-forward [34] or amplify-and-forward relaying [7], both already demonstrated in practical mmWave system design [7], [38]. In this work, we emulate the amplify-and-forward mode by ignoring the time-division-multiple-access overhead across the two hops. About the potential decode-and-forward mode, the signaling protocols for establishing two-hop relay links have already been standardized in 802.11ad [4]. However, problems such as whether to use relay and when to switch remain open. RoMil enables such decision making, as it can predict the individual link qualities (AP-client vs. AP-relay-client) and proactively switch to the relay mode when needed.

Implementation of RoMil modules. We implement RoMil's major design components (*i.e.*, environment reconstruction, client tracking, path planning algorithms, and also the ray-tracer) in Matlab, which run on the relay's NUC. To facilitate *real-time path planning*, we offload the computation of offline sensing (Sec.IV), backup set determination (Sec. VI-D) and E-index computation (Sec. VI-A) on a PC server, and feed the results to the AP and relay in the form of static data structures and lookup tables. For instance, after environment learning, RoMil computes the E-index $\eta(i,j,u,v)$ for all pairs of relay $r(i,j)$ and client $c(u,v)$ offline, which avoids the notoriously time-consuming ray-tracing [15]. Then at running stage, only efficient table-look-up and basic arithmetic operations are needed. The overall *latency* is less than 10ms for RoMil making each movement decision in our current implementation, and can be further reduced if RoMil is incorporated and runs inside low-layer NIC driver module. A similar offline caching mechanism is implemented for client localization (see Sec. V). Recall that the client localization is based on the beacon RSS measurements at 802.11ad's BI intervals (100 ms), which is fast enough for real-time decision making.

VIII. EXPERIMENTAL EVALUATION

A. Micro Benchmarks

1) Environment Learning: **Signal path estimation.** We first verify the effectiveness of BCS-CM and SMIC in isolating multiple NLoS/LoS signal paths and estimating their geometries. We set up 100 Tx-Rx pairs randomly located in the experimental space (*i.e.*, Fig. 2, unless otherwise noted) and get the ground-truth from measurements using a software radio with a 3° horn antenna. Fig. 14 plots the CDF of AoA estimation error (we omit AoD as the results are similar). We have two major observations: *(i)* RoMil extracts up to 4 paths before its SMIC iteration terminates. This echoes previous measurement insights that only $3 \sim 5$ major paths exist in the typical indoor environment due to channel sparsity [15], [39]. *(ii)* RoMil can accurately estimate signal paths, with a small mean error $1.64°$ across all paths. A further examination reveals that the error tends to be higher for weaker paths due to residual inter-path interference. However, even for the 4_{th} paths immersed under the previous three, the average error is only $7.31°$.

AP localization. To verify RoMil's AP localization method, we place the AP to 10 random locations with arbitrary orientations. Fig. 15 shows the mean error and std. As the robot roams to more points to collect more AoA/AoD samples, the AP sensing errors keep decreasing. Even with 5 sampling points, RoMil can already estimate the AP's location (orientation) with a small mean error of 5 cm (1°). Converging to this small error takes only around 1 minute.

Reflector reconstruction. To validate the reflector reconstruction, we let RoMil relay scan the environment following Sec. IV, and depict the estimated reflecting points along with the robot-generated floor map in Fig. 16. We note that: *(i)* The positions of reflecting points closely match the ground truth. The mean error is within 0.38m (Table I), and below 0.25m for strong reflectors (*i.e.*, walls). *(ii)* The estimated reflection loss well matches the material properties.

2) Client Tracking: **Accuracy of client tracking.** We now let a client user move continuously along a randomly-generated trajectory, and the relay navigates itself according to the path planning algorithm (Sec. VI). We repeat the experiment across 10 trajectories, and pick 10 equally-spaced

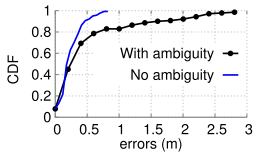

Fig. 17. CDF of client tracking errors.

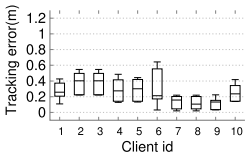

Fig. 18. Impact of rotation on client tracking.

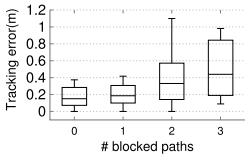

Fig. 19. Impact of blockage on client tracking.

positions along each trajectory to verify the client tracking accuracy. From the results in Fig. 17, we observe that: *(i)* The location ambiguity significantly undermines localization accuracy. While 70% points have an error of less than 0.5m, there exist points with up to 3m error. *(ii)* Fortunately, RoMil's ambiguity-removing mechanism effectively removes outliers and brings the average error down to 0.23m.

Robustness to client rotation and blockage. Using the same setup as above, we let the client rotate in steps of 30° at each location. The box plot in Fig. 18 shows the client tracking error, at 10%, 25%, 50%, and 90%. We see that the 90-th errors are below 0.62m and median below 0.4m, regardless of the client's position and orientation. We further select 10 client locations that have 4 paths between the relay, and intentionally block 1 to 3 paths. Fig.19 plots the localization errors. Though the average location error keeps increasing, it remains less than 0.5m even when 3 paths are blocked. The experiments validate that *RoMil's client tracking ability is resilient to user rotation dynamics, and does not require the existence of a LoS path as in traditional phased-array localization schemes [40].*

3) Path Planning: **How well does E-index model spatial performance?** Recall that E-index is a probabilistic metric, intended to reflect potential link performance. We now evaluate it against the ground-truth link bitrate. Specifically, we select 100 relay-client pairs with random locations. For each pair, we first rotate the client to 20 random directions, and then block the client 20 times with different path combinations. For each run, we measure the link RSS and map it to 802.11ad bitrate as in [4], [12]. Then we compute the average bitrate over all rotation and blockage settings for each client, and plot it against the client's E-index. The results (Fig. 20) show that: *(i)* The RSS fluctuates even for a fixed E-index, which roots from the probabilistic entropy-like definition of E-index. *(ii)* A clear positive logarithmic-correlation holds between E-index and RSS, as expected from the log term in Eq. (9). Therefore, *E-index can indeed quantitatively represent relay performance*.

Moreover, we compare E-index with angular spread [41], another metric used to model power angular profiles. In particular, we compute the angular spread value under the same

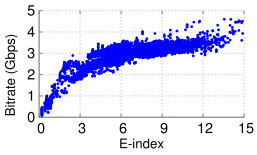

Fig. 20. E-index v.s. bitrate.

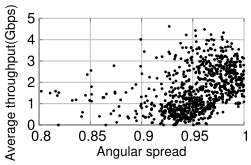

Fig. 21. Angular spread v.s. bitrate.

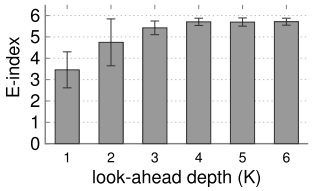

Fig. 22. Impact of look-ahead steps.

setup, and give the mapping between them and the average bitrates Fig. 21. We can observe that angular spread is less discriminating: for each single angular spread value, the range of bitrate variation is much wider. For instance, the bitrate ranges from 0 to 5 Gbps, even for a very high angular spread value of 0.95. The reason lies in that E-index better balance the impact of the sum RSS and angular distribution of multi-path signals, while the angular spread emphasize the latter, according to its definition in [41].

Relay path optimality. We run RoMil's path planning algorithm over the aforementioned 10 client trajectories. For each trajectory, we examine the relay performance by comparing the mean E-index (*i.e.*, over all points along the trajectory) under different look-ahead depths. Fig. 22 shows that: *(i)* E-index increases from 3.4 to 5.6 when look-ahead depth K increases from 1 to 6, because look-ahead offers more information especially about the abrupt environmental changes, so that RoMil can prepare in advance to avoid link outage. *(ii)* More importantly, the gain quickly saturates as look-ahead depth increases to 3. The finding further corroborates the locality effect of relay performance (Sec. VI): the optimal relay position (corresponding to the next client position) is often close by. So, even with a small look-ahead depth, *RoMil can achieve high performance while avoiding the exponential computational complexity, which paves the way for real-time relay path planning*.

Impact of moving speed. We repeat the above 10-trajectory experiment, but vary the robot's speed from 0.1 to 1 (relative to the client's speed 0.8m/s). For comparison, we also compute the performance of Oracle(E-index) and Oracle(throughput), which assumes an infinite-speed relay that can immediately move to the position with the maximum E-index and throughput, respectively. Fig. 23 shows that: although a faster relay may reach the optimal position sooner, the benefit converges at a speed of 0.6 owing to the locality property. Therefore, *the robot relay does not need to follow the client's speed. It can*

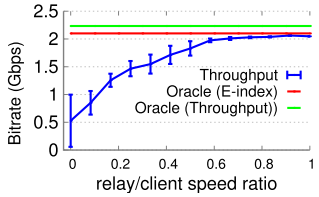

Fig. 23. Effect of relay moving speed.

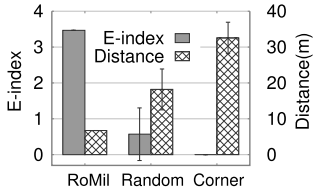

Fig. 24. Effectiveness of backup set.

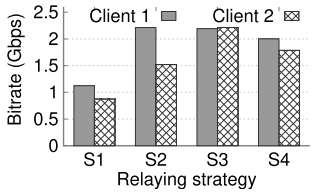

Fig. 25. One relay serving two close-by clients.

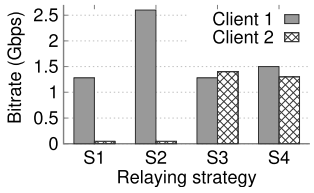

Fig. 26. One relay serving two separated clients.

keep near/in the optimal relay zone even when it moves much more slowly.

4) Effectiveness in Resolving the Cold-Start Issue: We compare RoMil's backup set strategy with two baselines, which put the relay randomly or at corners following common practices in Wi-Fi deployment. Here we use 3 backup positions. We see from the results (Fig. 24) that: *(i)* RoMil's backup set achieves $5\times$ higher E-index than random, whereas the corner approach fails as it always leads to blind zones. *(ii)* The traversal length of is about 1/3 and 1/4 compared with random and corner. The result implies that *RoMil's cold-start time is very short, i.e., only multiple seconds given a common robot moving speed of 0.5m/s* [33].

5) Multiple Clients/Relays Support: **One relay serving multiple clients.** We evaluate the multi-client scenario through two representative cases: two clients u_1 and u_2 moving as a cluster ($\leq 1m$ separation along their trajectories), and moving independently ($\geq 10m$ separation). We compare 4 relaying strategies, which determine the optimal relay positions using Alg. 2 but with different optimization objectives: no relay (denoted as S1); relay maximizing E-index of u_1 or u_2 (strategy S2 and S3); maximizing the sum of two users' E-index (strategy S4). From Fig. 25 and Fig. 26, we observe that: *(i)* In cluster case, strategy S2 and S3 achieve similar performance, which implies that one relay suffices for scenarios where co-resident users tend to cluster in space. *(ii)* In separation case, prioritizing user with higher link quality

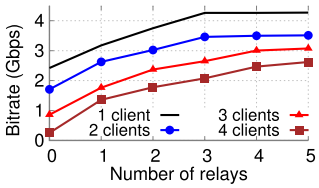

Fig. 27. Multiple relays serving multiple clients.

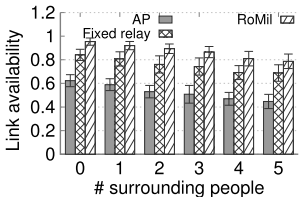

Fig. 28. Link availability.

(*i.e.*, u_1) will lead to severe unfairness in S2, whereas S3 serving weaker user (u_2) achieves similar effect The result roots from the fact that E-index approximates proportional fairness by the logarithmic operation in its entropy-like definition in Eq. (9).

Multiple relays serving multiple clients. We use the ray-tracing engine to examine RoMil's scalability. We incrementally add clients to random positions, and accordingly add relays to locations with largest sum E-index. The results (Fig. 27) show that *(i)* The average bitrate of client group tends to decline as more clients join, because the relays' positions become suboptimal as the clients spread out. *(ii)* Given the same number of clients, the throughput gain becomes marginal as more relays join. For instance, for the 4-client group, the first relay contributes to 44.7% of the throughput gain in a 5-relay setup. The result implies that *one relay can already harvest significant benefit from RoMil, and may suffice for home environment where cost is a major concern.*

B. System Level Evaluation

Now we evaluate RoMil's performance end to end.

Link availability. We now conduct a system-level evaluation of RoMil in the typical indoor scenario of Fig. 2, with one user holding the client device, while up to 5 other people walking around causing dynamic blockage. We compare RoMil with two baselines: AP-only, and fixed-relay (placed opposite to the AP as in Sec. II). We first evaluate link availability over 10 random client trajectories. *Link availability* is defined as the percentage of time when throughput exceeding a threshold T (here defined as half of the maximum throughput of our 802.11ad radios). The results (Fig. 28) show that RoMil achieves 87.2% availability on average across all the setup, in comparison to 52.8% and 75.5% for AP-only and fixed-relay, respectively. In particular, RoMil's link availability is around 95.4% when no other people exist, achieving a nearly seamless coverage for the client.

We emphasize that the key merit of RoMil lies in the ability of eliminating *worst case performance* (link outages and disconnections), which is the bottleneck to user QoS. Such cases mostly happen when the client moves into a blind spot for the AP or fixed-relay. The results in Fig. 29 validate our intuition: for the 3 client positions with lowest performance, RoMil can increase link availability from 35% to 95% with the client alone, and to 88% even when two other active people.

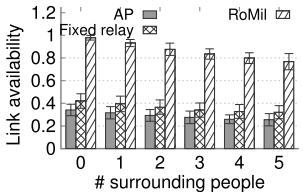

Fig. 29. Performance of worst-case client locations.

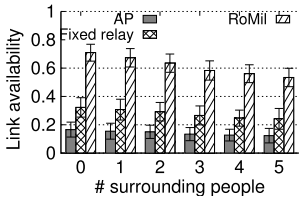

Fig. 30. Link availability in the complicated lab env.

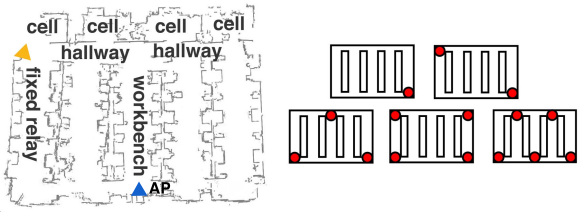

Fig. 31. A larger lab and multi-AP placement.

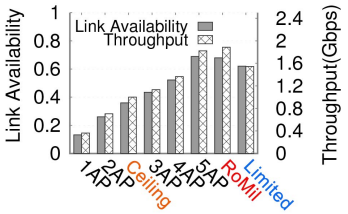

Fig. 32. Performance of RoMil vs. multi-AP.

We also repeat the link availability test in a larger and more complicated $14 \times 16\ m^2$ lab space (Fig. 31), with 4 half-open cells and 6 arrays of workbenches that can easily block the mmWave links. We can observe from the results in Fig. 30 that *even in a challenging environment, RoMil demonstrates superior performance. It improves link availability by more than 2×, compared with the other two solutions.*

Performance comparison with multiple fixed APs. We compare RoMil against a multi-AP solution. In particular, we increasingly deploy from 1 AP to 5 APs in the lab space, which are placed at corners or wall-mounted with complementary FoVs (Fig. 31). Measurement results (Fig. 32) show that: RoMil's link availability and throughput is comparable to 5-AP. Even when the robot moves in a highly constrained region (within 0.5m against walls), RoMil's performance (labeled "limited") is still much better than 4-AP, and close to 5-AP. In addition, we also examine the performance of another conventional 'Ceiling' deployment, *i.e.*, mounting APs in the center ceiling of the room. We deploy 3 back-to-back APs to form a 360° coverage (each AP with 170°). From Fig. 32, we observe that the 'ceiling' deployment is worse than the corner 3-AP deployment, because the APs' FoV are less complimentary. For instance, if a client device faces to the wall (*i.e.*, the opposite to the room center), there is no AP

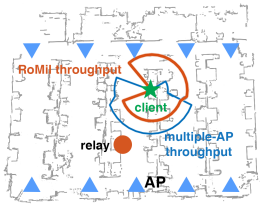

Fig. 33. Multi-AP unable to eliminate blind angles.

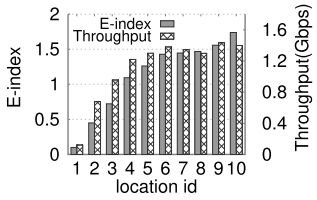

Fig. 34. E-index vs. field measured throughput.

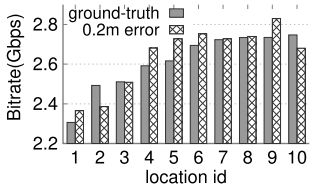

Fig. 35. Impact of client localization error.

to provide line-of-sight signal paths to the client. Note that the observation corroborates previous findings in [42].

We also showcase an extreme example in Fig. 33, where 10 APs are deployed, and a client is located near the corner of a workbench. The polar graphs show the circular throughput for multi-AP (blue curve) and RoMil (orange curve), respectively. We can observe that even 10 APs cannot provide a stable link due to the existence of blind angles, whereas RoMil achieves a near-omnidirectional coverage.

C. RoMil Robustness Evaluation

Impact of environment mapping error. The foregoing experiments demonstrate that the environment sensing may miss some smaller reflectors or scatters (Fig. 16). Here we evaluate the impact of such imperfectness by comparing the link performance predicted by RoMil and from the actual measurement. We first randomly choose 10 locations in the ray-tracer and sort them in ascending order of their E-index. Then we measure the actual mean throughput as the client rotates 360° at each location. We observe from Fig. 34 that despite minor fluctuation due to imperfect environment construction, the trends of E-index and that of ground-truth throughput are highly consistent. The result validates the *strong resilience of RoMil in predicting the relay performance*, and echoes the well-known fact that a few major reflectors and obstacles dominate mmWave performance [15], [39].

Impact of client tracking error. We evaluate the effect of client tracking error by randomly choosing a client location c_1 and 10 relay locations, and ranking the measured bitrate. Then we choose a client c_2 which is 0.2m (*i.e.*, the average client tracking error of RoMil) away from c_1, and repeat the measurement. The comparison in Fig. 35 clearly shows that a location displacement of 0.2m does not hamper RoMil's relay performance prediction. To understand how much error RoMil can tolerate, we intentionally increase the location error, and found that the average bitrate deviation is insignificant

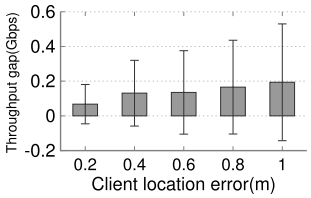

Fig. 36. Impact of client loc. err on sys. throughput.

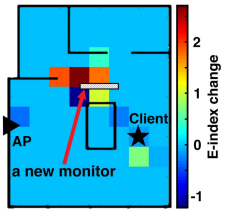

Fig. 37. A showcase of impact of environment change on E-index.

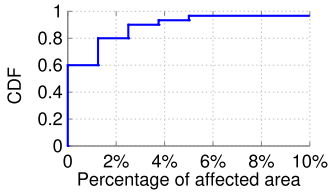

Fig. 38. CDF of affected grids by environment change.

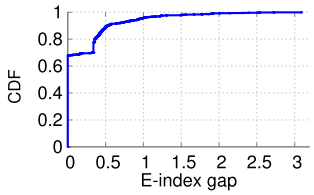

Fig. 39. CDF of E-index gap caused by environment change.

(Fig. 36). However, the std. increases fast, indicating that large deviation can occur when a client is wrongly located across multiple rooms. Fortunately, the case rarely happens under RoMil's small tracking error.

Impact of environment change The environment may change (*e.g.*, moving a table/chair or adding a PC monitor) after RoMil's initial sensing stage. To investigate the impact, we first showcase in Fig. 37 the change of E-index at all locations after a new monitor (0.6m×0.4m, reflectivity 0.8) is added. We can observe that only few close-by locations have been impacted noticeably (with a E-index variation ≥ 0.5), due to the inherent spatial channel sparsity. We plot the CDF of ratios of affected locations, when we move the reflector to 30 random locations, in Fig. 38. Clearly, less than 2.5% locations will be affected for more than 90% cases.

We then let a client user walk around and meanwhile change the environment randomly for 30 times by adding reflectors with different reflectivity. We derive the best relay positions along the client user's trajectory, with and without considering the environment change, and plot the CDF of E-index/throughput gaps caused by environment change in Fig. 39 and Fig. 40. We observe that the E-index gap is less than 0.5 and the throughput gap is lower than 300 Mbps (only around 12.5% of the peak throughput) for more than 90% of client user moving duration. To sum up, *RoMil is robust to most daily indoor environment changes*. Moreover, it can

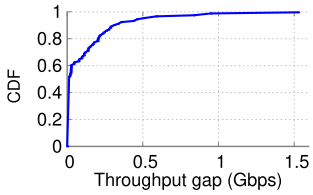

Fig. 40. CDF of RoMil performance gap caused by environment change.

re-profile the environment when it observes low performance likely due to significant and permanent change.

IX. Discussion

From 2-D to 3-D relay. RoMil mainly exploits the relay's movement/rotation on the horizontal plane, and exploits reflectors at similar height. The premise is that the clients usually have limited mobility along the vertical direction. In fact, COTS 60 GHz phased-arrays are also designed to offer a narrower elevational FoV (*e.g.*, 40° on QCA 6310), and more steerability and wider FoV on the horizontal plane. More versatile robots (*e.g.*, mechanical lifter or drones) hold potential to reconstruct 3-D environment and thus harness ceiling/floor reflection to achieve better relay performance. One related issue is to provide relay service in outdoor environment with 3D space. Unlike indoor scenario, the blockage issue may become more severe due to lack of reflectors and alternative reflection paths to the clients. One solution is to deploy more relays, which operate in a coordinated way to provide seamless coverage even under blockage. In fact, there are some other research effort on this topic, please refer to a recent work [43] and references therein.

System extension. RoMil involves only one AP associated with the robotic relay, and we focus on solving challenges of client tracking and relay path planning. For an extended scenario involving multiple APs and even multiple relays, new challenges will arise including AP switching and movement coordination among relays. We leave such exploration for future work.

Power sustainability. The Create 2 robot we use has a rated power consumption of 33 W. Its battery can be recharged in 3 hours and sustain 3.5 hours under continuous movement and sweeping. The 60 GHz radio introduces an extra power consumption of ∼2.3 W [44], [45], only 7% of the robot's own power. Moreover, unlike the cleaning mode, RoMil's robot relay does not require constant movement, and thus saves major power. In our system-level tests, the RoMil relay can run for about 6 hours after a full charge, with a NUC payload of 0.8 kg and the robot itself 3.6 kg. We expect longer running time if the 60 GHz radios are integrated inside the robot and better power management schemes are incorporated. We leave such optimization for future work.

Application extension: while we mainly focus on the instantaneous relaying mechanism in RoMil, it can also be extended into a store-and-forward framework, *i.e.*, receiving packets from the AP and delivering them to users located in a different room, analogous to postal service. We have two notes on such extension: *(i)* In postal-like service, the RoMil robot does not need to track and follow users in real-time. Instead, it can stay close with the AP to receive the target data (*e.g.*, a file or a movie), and then roams to locate the client and deliver the data. We note that such client localization ability is already supported in RoMil, which is originally designed for solving the "cold-start" issue. Please refer to details in Sec. 6.4.

(ii) To accomplish the full postal-like service, some delay-tolerant network (DTN) protocols or application-level relaying protocols should be supported by the AP, relay and client users. We are aware that rich literature exists on DTN protocol design [46], among which deciding and incorporating the most suitable one for RoMil should be the major task.

X. Related Work

Millimeter-wave networking systems. Lack of coverage and stability is a major issue for mmWave networks, as validated in many measurement studies [12], [47], [48]. Substantial research [16], [21], [39], [49], [50] focused on efficient beam steering methods to rapidly recover from mobility/blockage disruptions. For example, BBS [49] and MUST [21] exploit side-channel information from co-located WiFi module. Beamspy [39], Oscan [51] and other similar systems [16], [37] harness the channel sparsity to predict best beam without scanning. E-Mi [15] leverages environment maps to predict reflection paths. Yet even perfect beam steering cannot overcome the blind zones due to limited FoV [6]. Different from the robotic solution in this paper, a most recent work [52] explores an array of co-located static phased arrays (APA) architecture with coverage-enhancing mechanisms (*e.g.*, joint array and beam selection, co-phasing signal boost) to approximate WiFi-like omni-directional coverage. The benefits of mmWave relaying have been verified theoretically [53], [54], and through preliminary measurements [38]. *Static* mmWave relays or APs have been exploited [6], [7] to overcome the limited FoV. We have provided experimental evidence to show the limitations of such systems, and the advantages of an autonomous mobile relay.

Environment learning and localization. To sense or image surrounding reflectors, existing systems either move a pair of mmWave Tx/Rx radios following a deliberately designed trajectory to scan a specific reflector [55], [56], or place radios at specific site-survey points to sense the mmWave channel [6], [15]. In particular, E-Mi [15] uses a multi-path resolution framework to estimate the AoA/AoD of signal paths. But it relies on both RSS and phase measurements on a custom-built software radio, due to lack of coherent phase information on COTS devices. In addition, it entails non-trivial human intervention to execute the site measurement. In contrast, RoMil integrates a robot's own sensing capabilities with mmWave sensing mechanisms, and uses RSS measurement alone on low-profile COTS devices to realize autonomous environment mapping. This kind of light weight RSS-based tracking and environment estimation can also benefit indoor/outdoor localization.

Recent work also proposed device tracking methods to speed up mmWave beam alignment [57]–[59]. As inputs for the path planning, RoMil's AP/client location sensing module differs from previous localization solutions, in that it leverages precise motion control and diverse beam patterns (*i.e.*, BCS) of the robotic mmWave relay. RoMil accurately senses both location and orientation using COTS mmWave radios which can only measure RSS. It does not need phase measurement, and works even when the LoS path is blocked.

Path planning and robotic networks. Path planning has been extensively investigated [18], [19] in robotics domain. The classical A^* algorithm [29] navigates a robot to destination while avoiding obstacles. D^* and D^*-lite [30], [60] further handle cases of moving destination or dynamic environment. Other refined algorithms [61], [62] attempted to reduce planning latency. Path planning has also been investigated in robot-driven omnidirectional radio networks [17], [18]. Whereas RoMil shares similar spirit, the objective of robotic mmWave relay differs in that the planned path needs to guarantee the overall statistical link performance comprised of all *signal propagation paths*, instead of simply being the optimal geometrical path towards a number of points of interest. Moreover, mmWave's strong dependence on environment and thus the dynamic roadmap make previous path planning mechanisms infeasible. Essentially, RoMil solves a set of unique problems in the intersection between mmWave networking and robotics.

XI. Conclusion

This paper envisions the proliferation of consumer-grade robots, and proposes a robotic mmWave system, RoMil, to achieve seamless mmWave coverage in complicated home or office environment. Through RoMil, we have demonstrated the feasibility of leveraging the autonomous motion of a robot to reverse engineer the geometrical properties of wireless channel. We have also explored new robotic path planning solutions that navigate the robot within radio environment, instead of physical environment alone, to facilitate network performance. We believe RoMil hints on a new direction that embraces robotic intelligence into wireless network design and operations.

References

[1] S. Singh, R. Mudumbai, and U. Madhow, "Interference analysis for highly directional 60-GHz mesh networks: The case for rethinking medium access control," *IEEE/ACM Trans. Netw.*, vol. 19, no. 5, pp. 1513–1527, Oct. 2011.

[2] W. Zhang, X. Zhou, L. Yang, Z. Zhang, B. Y. Zhao, and H. Zheng, "3D beamforming for wireless data centers," in *Proc. 10th ACM Workshop Hot Topics Netw. (HotNets)*. New York, NY, USA: ACM, 2011.

[3] Y. Cui *et al.*, "Diamond: Nesting the data center network with wireless rings in 3D space," in *Proc. NSDI*, 2016, pp. 657–669.

[4] *IEEE Standard for Information Technology–Telecommunications and Information Exchange Between Systems–Local and Metropolitan Area Networks–Specific Requirements-Part 11: Wireless LAN Medium Access Control (MAC) and Physical Layer (PHY) Specifications Amendment 3: Enhancements for Very High Throughput in the 60 GHz Band*, IEEE Standard 802.11ad-2012, IEEE Standards Association, 2012.

[5] R. Sun. (2017). *IEEE 802.11 TGay Use Cases 11-15/0625r7*. [Online]. Available: https://mentor.ieee.org/802.11/dcn/15/11-15-0625-07-00ay-ieee-802-11-tgay-usage-scenarios.pptx

[6] T. Wei and X. Zhang, "Pose information assisted 60 GHz networks: Towards seamless coverage and mobility support," in *Proc. 23rd Annu. Int. Conf. Mobile Comput. Netw. (MobiCom)*, 2017, pp. 42–55.

[7] O. Abari, D. Bharadia, A. Duffield, and D. Katabi, "Enabling high-quality untethered virtual reality," in *Proc. NSDI*, 2017, pp. 531–544.

[8] MIT-tr. (2018). *Robots are Becoming Ready to Work Among us*. [Online]. Available: http://www.technologyreview.com/view/522646/robotsare-becoming-ready-to-work-among-Us

[9] iRobot. (2018). *iRobot Roomba*. [Online]. Available: http://www.irobot.com/us/learn/home/roomba.aspx

[10] (2013). *Rise of the Telepresence Robots*. [Online]. Available: https://www.forbes.com/sites/parmyolson/2013/06/27/rise-of-the-telepresence-robots/

[11] 2017. *Telepresence Robots Market Worth $8 Billion by 2023*. [Online]. Available: https://www.prnewswire.com/news-releases/telepresence-robots-market-worth-8-billion-by-2023-says-a-new-research-at-reportsnreports-629894233.html

[12] S. Sur, V. Venkateswaran, X. Zhang, and P. Ramanathan, "60 GHz indoor networking through flexible beams: A link-level profiling," in *Proc. ACM SIGMETRICS Int. Conf. Meas. Modeling Comput. Syst. (SIGMETRICS)*, 2015, pp. 71–84.

[13] M. Minelli, M. Ma, M. Coupechoux, J.-M. Kelif, M. Sigelle, and P. Godlewski, "Optimal relay placement in cellular networks," *IEEE Trans. Wireless Commun.*, vol. 13, no. 2, pp. 998–1009, Feb. 2014.

[14] F. El-Moukaddem, E. Torng, and G. Xing, "Mobile relay configuration in data-intensive wireless sensor networks," *IEEE Trans. Mobile Comput.*, vol. 12, no. 2, pp. 261–273, Feb. 2013.

[15] T. Wei, A. Zhou, and X. Zhang, "Facilitating robust 60 GHz network deployment by sensing ambient reflectors," in *Proc. USENIX NSDI*, 2017, pp. 213–226.

[16] M. E. Rasekh, Z. Marzi, Y. Zhu, U. Madhow, and H. Zheng, "Noncoherent mmWave path tracking," in *Proc. 18th Int. Workshop Mobile Comput. Syst. Appl.*, Feb. 2017, pp. 13–18.

[17] Y. Yan and Y. Mostofi, "Efficient clustering and path planning strategies for robotic data collection using space-filling curves," *IEEE Trans. Control Netw. Syst.*, vol. 4, no. 4, pp. 838–849, Dec. 2017.

[18] C. Goerzen, Z. Kong, and B. Mettler, "A survey of motion planning algorithms from the perspective of autonomous UAV guidance," *J. Intell. Robotic Syst.*, vol. 57, nos. 1–4, pp. 65–100, Jan. 2010.

[19] J.-C. Latombe, *Robot Motion Planning*. Norwell, MA, USA: Kluwer, 1991.

[20] Xiaomi. (2018). *Mi Robot Vacuum Cleaner*. [Online]. Available: https://www.amazon.com/Xiaomi-Cleaner-Guidance-Powerful-Planning/dp/B01MU4WAUI

[21] S. Sur, I. Pefkianakis, X. Zhang, and K.-H. Kim, "WiFi-assisted 60 GHz wireless networks," in *Proc. 23rd Annu. Int. Conf. Mobile Comput. Netw. (MobiCom)*, 2017, pp. 28–41.

[22] Z. Marzi, D. Ramasamy, and U. Madhow, "Compressive channel estimation and tracking for large arrays in mm-wave picocells," *IEEE J. Sel. Topics Signal Process.*, vol. 10, no. 3, pp. 514–527, Apr. 2016.

[23] MATLAB. (2018). *Corrcoef*. [Online]. Available: https://ww2.mathworks.cn/help/matlab/ref/corrcoef.html?lang=en

[24] D. Tse and P. Viswanath, *Fundamentals of Wireless Communication*. New York, NY, USA: Cambridge Univ. Press, 2005.

[25] W.-L. Shen, K. C.-J. Lin, S. Gollakota, and M.-S. Chen, "Rate adaptation for 802.11 multiuser MIMO networks," *IEEE Trans. Mobile Comput.*, vol. 13, no. 1, pp. 35–47, Jan. 2014.

[26] Y. Guo, Z. Wang, M. Li, and Q. Liu, "Machine learning based mmWave channel tracking in vehicular scenario," in *Proc. IEEE Int. Conf. Commun. Workshops (ICC Workshops)*, May 2019, pp. 1–6.

[27] A. Alkhateeb, I. Beltagy, and S. Alex, "Machine learning for reliable mmWave systems: Blockage prediction and proactive handoff," in *Proc. IEEE Global Conf. Signal Inf. Process. (GlobalSIP)*, Nov. 2018, pp. 1055–1059.

[28] D. J. C. MacKay, *Information Theory, Inference and Learning Algorithms*. New York, NY, USA: Cambridge Univ. Press, 2002.

[29] P. Hart, N. Nilsson, and B. Raphael, "A formal basis for the heuristic determination of minimum cost paths," *IEEE Trans. Syst. Sci. Cybern.*, vol. 4, no. 2, pp. 100–107, Jul. 1968.

[30] A. Stentz, "Optimal and efficient path planning for partially-known environments," in *Proc. IEEE Int. Conf. Robot. Autom.*, vol. 4, May 1994, pp. 3310–3317.

[31] J. Han, M. Kamber, and J. Pei, *Data Mining: Concepts and Techniques*, 3rd ed. San Mateo, CA, USA: Morgan Kaufmann, 2011.

[32] Intel. (2018). *Intel NUC Mini PCs*. [Online]. Available: https://www.intel.com/content/www/us/en/products/boards-kits/nuc/mini-pcs.html

[33] iRobot Inc. (2018). *iRotot Create 2 Programmable Robot*. [Online]. Available: http://www.irobot.com/About-iRobot/STEM/Create-2.aspx

[34] Qualcomm Inc. (2015). *Qualcomm VIVE 802.11ad*. [Online]. Available: https://www.qualcomm.com/products/vive/11ad,

[35] C. Rowell and E. Y. Lam, "Mobile-phone antenna design," *IEEE Antennas Propag. Mag.*, vol. 54, no. 4, pp. 14–34, Aug. 2012.

[36] J. Palacios, D. Steinmetzer, A. Loch, M. Hollick, and J. Widmer, "Adaptive codebook optimization for beam training on off-the-shelf IEEE 802.11ad devices," in *Proc. 24th Annu. Int. Conf. Mobile Comput. Netw. (MobiCom)*, Oct. 2018, pp. 241–255.

[37] D. Steinmetzer, D. Wegemer, M. Schulz, J. Widmer, and M. Hollick, "Compressive millimeter-wave sector selection in off-the-shelf IEEE 802.11ad devices," in *Proc. 13th Int. Conf. Emerg. Netw. Exp. Technol.*, Nov. 2017, pp. 414–425.

[38] S. K. Saha, L. Sun, and D. Koutsonikolas, "Improving connectivity, coverage, and capacity in 60 GHz indoor WLANs using relays," in *Proc. Workshop Wireless Students, Students, Students (S3)*, 2015, pp. 35–37.

[39] S. Sur, X. Zhang, P. Ramanathan, and R. Chandra, "BeamSpy: Enabling robust 60 GHz links under blockage," in *Proc. USENIX NSDI*, 2016, pp. 193–206.

[40] J. Xiong and K. Jamieson, "Arraytrack: A fine-grained indoor location system," in *Proc. NSDI*, 2013, pp. 71–84.

[41] H. Xu, V. Kukshya, and T. S. Rappaport, "Spatial and temporal characteristics of 60-GHz indoor channels," *IEEE J. Sel. Areas Commun.*, vol. 20, no. 3, pp. 620–630, Apr. 2002.

[42] G. Bielsa, A. Loch, I. Tejado, T. Nitsche, and J. Widmer, "60 GHz networking: Mobility, beamforming, and frame level operation from theory to practice," *IEEE Trans. Mobile Comput.*, vol. 18, no. 10, pp. 2217–2230, Oct. 2019.

[43] Y. Huo, F. Lu, F. Wu, and X. Dong, "Multi-beam multi-stream communications for 5G and beyond mobile user equipment and UAV proof of concept designs," in *Proc. IEEE 90th Veh. Technol. Conf. (VTC-Fall)*, Sep. 2019, pp. 1–5.

[44] S. K. Saha, T. Siddiqui, D. Koutsonikolas, A. Loch, J. Widmer, and R. Sridhar, "A detailed look into power consumption of commodity 60 GHz devices," in *Proc. IEEE 18th Int. Symp. World Wireless, Mobile Multimedia Netw. (WoWMoM)*, Jun. 2017, pp. 1–10.

[45] S. K. Saha, D. G. Malleshappa, A. Palamanda, V. V. Vira, A. Garg, and D. Koutsonikolas, "60 GHz indoor WLANs: Insights into performance and power consumption," *Wireless Netw.*, vol. 24, no. 7, pp. 2427–2450, Feb.2017.

[46] Y. Li, P. Hui, D. Jin, and S. Chen, "Delay-tolerant network protocol testing and evaluation," *IEEE Commun. Mag.*, vol. 53, no. 1, pp. 258–266, Jan. 2015.

[47] Y. Zhu *et al.*, "Demystifying 60 GHz outdoor picocells," in *Proc. 20th Annu. Int. Conf. Mobile Comput. Netw. (MobiCom)*, 2014, pp. 5–16.

[48] T. Nitsche, G. Bielsa, I. Tejado, A. Loch, and J. Widmer, "Boon and bane of 60 GHz networks: Practical insights into beamforming, interference, and frame level operation," in *Proc. 11th ACM Conf. Emerg. Netw. Exp. Technol. (CoNEXT)*, 2015, pp. 1–13.

[49] T. Nitsche, A. B. Flores, E. W. Knightly, and J. Widmer, "Steering with eyes closed: mm-wave beam steering without in-band measurement," in *Proc. IEEE Conf. Comput. Commun. (INFOCOM)*, Apr. 2015.

[50] M. K. Haider and E. W. Knightly, "Mobility resilience and overhead constrained adaptation in directional 60 GHz WLANs: Protocol design and system implementation," in *Proc. 17th ACM Int. Symp. Mobile Ad Hoc Netw. Comput. (MobiHoc)*, 2016, pp. 61–70.

[51] A. Zhou, L. Wu, S. Xu, H. Ma, T. Wei, and X. Zhang, "Following the shadow: Agile 3-D beam-steering for 60 GHz wireless networks," in *Proc. IEEE Conf. Comput. Commun. (IEEE INFOCOM)*, Apr. 2018, pp. 2375–2383.

[52] S. Wang, J. Huang, X. Zhang, H. Kim, and S. Dey, "X-array: Approximating omnidirectional millimeter-wave coverage using an array of phased arrays," in *Proc. ACM MobiCom*, Sep. 2020, pp. 1–14.

[53] L. Kong, L. Ye, F. Wu, M. Tao, G. Chen, and A. V. Vasilakos, "Autonomous relay for millimeter-wave wireless communications," *IEEE J. Sel. Areas Commun.*, vol. 35, no. 9, pp. 2127–2136, Sep. 2017.

[54] S. Kwon and J. Widmer, "Relay selection for mmWave communications," in *Proc. IEEE 28th Annu. Int. Symp. Pers., Indoor, Mobile Radio Commun. (PIMRC)*, Oct. 2017, pp. 1–6.

[55] Y. Zhu, Y. Zhu, B. Y. Zhao, and H. Zheng, "Reusing 60 GHz radios for mobile radar imaging," in *Proc. 21st Annu. Int. Conf. Mobile Comput. Netw. (MobiCom)*, 2015, pp. 103–116.

[56] Y. Zhu, Y. Yao, B. Y. Zhao, and H. Zheng, "Object recognition and navigation using a single networking device," in *Proc. 15th Annu. Int. Conf. Mobile Syst., Appl., Services*, Jun. 2017, pp. 265–277.

[57] A. Olivier, G. Bielsa, I. Tejado, M. Zorzi, J. Widmer, and P. Casari, "Lightweight indoor localization for 60-GHz millimeter wave systems," in *Proc. 13th Annu. IEEE Int. Conf. Sens., Commun., Netw. (SECON)*, Jun. 2016, pp. 1–9.

[58] A. Loch, H. Assasa, J. Palacios, J. Widmer, H. Suys, and B. Debaillie, "Zero overhead device tracking in 60 GHz wireless networks using multi-lobe beam patterns," in *Proc. 13th Int. Conf. Emerg. Netw. Exp. Technol.*, Nov. 2017, pp. 224–237.

[59] J. Palacios, P. Casari, and J. Widmer, "JADE: Zero-knowledge device localization and environment mapping for millimeter wave systems," in *Proc. IEEE Conf. Comput. Commun. (IEEE INFOCOM)*, May 2017, pp. 1–9.

[60] X. Sun, W. Yeoh, and S. Koenig, "Moving target D* lite," in *Proc. AAMAS*, 2010, pp. 1–8.

[61] T. Ishida and R. E. Korf, "Moving-target search: A real-time search for changing goals," *IEEE Trans. Pattern Anal. Mach. Intell.*, vol. 17, no. 6, pp. 609–619, Jun. 1995.

[62] X. Sun, W. Yeoh, and S. Koenig, "Efficient incremental search for moving target search," in *Proc. IJCAI*, 2009, pp. 1–6

Anfu Zhou (Member, IEEE) received the B.S. degree from the Renmin University of China and the Ph.D. degree in computer science from the Institute of Computing Technology, Chinese Academy Sciences, in 2012. He is currently a Professor at the School of Computer Science, Beijing University of Posts and Telecommunications. His research interests include mobile computing, wireless networking, and the IoT systems.

Shaoqing Xu received the B.S. degree in computer science and technology from the Beijing University of Posts and Telecommunications in 2012, where he is currently pursuing the M.S. degree in computer science and technology. His research interest lies in wireless networks and mobile systems, with emphasis on simultaneous localization and mapping using mmWave radios.

Song Wang received the B.S. degree in the Internet of Things engineering from the Beijing University of Posts and Telecommunications in 2018. He is currently pursuing the M.S. degree with the Electrical and Computer Engineering (ECE) Department, University of California at San Diego. His research interest lie in wireless networking with emphasis on seamless mmWave communication applications.

Jingqi Huang received the B.E. degree in the Internet of Things engineering from BUPT in 2018. She is currently pursuing the M.S. degree in electrical and computer engineering with the University of California at San Diego. Her research interest lies in wireless network and mobile computing, with emphasis on robust mmWave networking and applications.

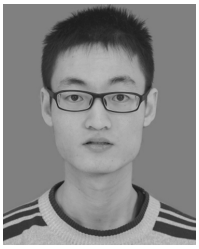

Shaoyuan Yang received the B.S. degree in the Internet of Things engineering from JLU in 2013. He is currently pursuing the M.S. degree in computer science and technology with the Beijing University of Posts and Telecommunications. His research interest lies in wireless networks and mobile systems, with emphasis on simultaneous localization and mapping.

Teng Wei received the B.S. degree from Shanghai Jiao Tong University in 2013. He is currently pursuing the Ph.D. degree with the Department of Electrical and Computer Engineering, University of Wisconsin-Madison. His research interest lies in wireless networks and mobile systems, with emphasis on ubiquitous wireless sensing for enabling new Internet of Things applications.

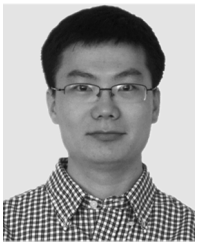

Xinyu Zhang (Associate Member, IEEE) received the Ph.D. degree from the University of Michigan in 2012. He is currently an Associate Professor at the Department of ECE, University of California at San Diego. Prior to joining UC San Diego, he was an Assistant Professor at the University of Wisconsin-Madison from 2012 to 2017. His research interest lies in wireless systems and ubiquitous computing. He was a recipient of the ACM MobiCom Best Paper Award in 2011, the NSF CAREER Award in 2014, and the Google Research Award in 2017.

Huadong Ma (Senior Member, IEEE) received the B.S. degree in mathematics from Henan Normal University, Xinxiang, China, in 1984, the M.S. degree in computer science from the Shenyang Institute of Computing Technology, Chinese Academy of Sciences, in 1990, and the Ph.D. degree in computer science from the Institute of Computing Technology, Chinese Academy of Sciences, Beijing, China, in 1995. From 1999 to 2000, he held a visiting position at the University of Michigan, Ann Arbor, USA. He was a Visiting Professor at The University of Texas at Arlington, TX, USA, from July 2004 to September 2004. He is currently a Chang Jiang Scholar Professor and the Executive Dean of the Institute of Networking Technology, Beijing University of Posts and Telecommunications (BUPT), China. He has published over 300 articles in prestigious journals (such as the IEEE/ACM TRANSACTIONS ON NETWORKING) or conferences (such as ACM MobiCom/MM and the IEEE INFOCOM) and five books. His current research focuses on multimedia system and networking, the Internet of Things, and sensor networks. He was awarded the Natural Science Award of the Ministry of Education, China, in 2017. He was a recipient of the 2019 Prize Paper Award of the IEEE TRANSACTIONS ON MULTIMEDIA, the 2018 Best Paper Award from the IEEE MULTIMEDIA, the Best Paper Award in IEEE ICPADS2010, and the Best Student Paper Award in IEEE ICME2016, for his coauthored articles. He received the National Funds for Distinguished Young Scientists in 2009. He serves as the Chair for ACM SIGMOBILE China. He is an Editorial Board Member of the IEEE TRANSACTIONS ON MULTIMEDIA, the IEEE INTERNET OF THINGS JOURNAL, ACM T-IoT, and MTAP.